Pergamon

Int. J. Heat Mass Transfer. Vol. 41, No. 16, pp. 2517–2528, 1998

Printed in Great Britain
0017-9310/98 $19.00+0.00

PII: S0017-9310(97)00311-6

Experimental and numerical study on natural convection from vertical plates with horizontal rectangular grooves

C. E. KWAK and T. H. SONG†

Department of Mechanical Engineering, Korea Advanced Institute of Science and Technology, Kusong-dong, Yusong-gu, Taejon, 305–701 Korea

(*Received* 29 *November* 1996 *and in final form* 26 *August* 1997)

Abstract—Natural convection from two-dimensional vertical plates with horizontal rectangular grooves was studied experimentally and numerically. A Mach–Zehnder interferometer was used in the experiment and the local Nusselt numbers at each groove surface (outer, bottom, inner, and top surfaces) were measured quantitatively from the interferograms. In some cases (grooves of some aspect ratios with low Rayleigh number), the total heat transfer rate from the grooved surface is even smaller than that from a flat plate in spite of the increased surface area; care should be practiced to avoid such cases. As revealed by the numerical analysis, for given conditions, secondary recirculation flows are usually found in the groove. They prevent the main flow from flowing into the groove. As they happen, the heat transfer rate at the inner surfaces is significantly smaller than that at the outer surface. The effect of Rayleigh number for each aspect ratio was studied. The results were summarized using the average Nusselt number vs. Rayleigh number correlations. The correlations may be used for selecting proper aspect ratio and dimension.

INTRODUCTION

The wide spread of modern electronic components and systems has been made possible by the rapid reduction of size with greater capability and processing rate. The distance between chips is becoming shorter and the integration rate of components is getting higher. The electric power consumption increases considerably while the size of electronic equipment diminishes. During the past 15 years, the power dissipation of chips in mainframe computers has increased almost 10 times. Although the chip size has also increased, the chip power density has been steadily increasing too. The approximate chip level heat flux or the power density has increased from 20 to 60 W cm^{-2} during the time. It is expected to reach 100 W cm^{-2} in the near future (Rymaszewski [1]).

Increase of the power density necessitates proper heat dissipation methods from the electronic components. Various cooling modules and the problems associated with electronic equipment cooling were well reviewed by Incropera [2].

The cooling methods may be classified into air-cooling, air–liquid hybrid cooling, indirect liquid cooling, and direct liquid cooling (immersion cooling). They can be also classified to natural convection, forced convection and boiling in accordance with the employed physical phenomena (Chu and Simons [3]).

The cooling system using natural convection has the advantage of low noise and high reliability. When used in air, it is generally limited to electronic components of low power density. High power density may be handled by immersion cooling, a liquid natural convection system for the next generation electronic circuits.

Grooved plate is one of the most popular geometries in extended surface cooling techniques and various heat transfer situations can be met depending on the flow and/or the groove orientations. The application of vertical grooves is an efficient way so far as the boundary layer thickness is thin enough to be treated as one from a vertical flat plate. When the groove orientation is horizontal, however, it proposes different flow situations and only limited number of researches have been reported in spite of the wide practical applications such as cylindrical pin fins (see Fig. 1). It gives impetus to this study and the case of natural convection from a vertical plate with horizontal rectangular grooves is studied in depth here.

Reviewing the related works, Fujii and Imura [4] experimentally investigated natural convection from a flat plate with arbitrary inclination and they suggested the correlation, $Nu = k(Gr\,Pr\cdot\cos\theta)^{1/4}$, for laminar region. Hung and Shiau [5] investigated local steady-state natural convection heat transfer in vertical parallel channel with a two-dimensional rectangular horizontal rib. By using experimental data, they found that the average Nusselt number correlates

† Author to whom correspondence should be addressed. Tel.: 00-82-42-869-3032. Fax: 00-82-42-869-3210. E-mail: thsong@sorak.kaist.ac.kr.

NOMENCLATURE

c_p	specific heat [J kg^{-1} K^{-1}]
Gr_w	Grashof number [$=(g\beta\Delta TW^3/\nu^2)$]
g	gravitational constant [9.81 m s^{-1}]
h	local heat transfer coefficient [W m^{-2} K^{-1}]
$\bar{h}_i$	average heat transfer coefficient for the i-th pitch ($q_i/W(T_w-T_\infty)$) [W m^{-2} K^{-1}]
H	depth of the groove in each case [m]
k	thermal conductivity [W m^{-1} K^{-1}]
L	total vertical length of the specimen [m]
n	refractive index of air
Nu_w	local Nusselt number (hW/k)
$\overline{Nu}_i$	average Nusselt number of the ith pitch of groove ($\bar{h}_iW/k$)
P	pressure [Pa]
P^*	dimensionless pressure [$=(P+\rho_\infty gy)/(\rho_\infty v^2/W^2)$]
Pr	Prandtl number [$=(\nu/\alpha)$]
q_i	total heat transfer rate from the ith pitch per unit depth [W m^{-1}]
q''	local heat flux [W m^{-2}]
Q	total heat transfer rate from the fin per unit depth [W m^{-1}]
Ra_w	Rayleigh number ($Gr_w \cdot Pr$)
T	temperature [K]
u	x-direction velocity [m s^{-1}]
v	y-direction velocity [m s^{-1}]
W	length of a pitch (W_1+W_2) [m]
W_1	width of groove [m]
W_2	width of the protrusion [m].

Greek symbols

α	thermal diffusivity [$=(k/\rho c_p)$]
β	thermal expansion coefficient [K^{-1}]
ΔT	temperature difference between the wall and the surrounding ($=T_w-T_\infty$)
θ	dimensionless temperature [$=(T-T_\infty)/(T_w-T_\infty)$]
ν	kinematic viscosity of the fluid [m^2 s^{-1}]
ρ	density of the fluid [kg m^{-3}].

Subscripts

g	groove
w	wall
∞	surrounding.

Superscript

*	dimensionless quantity.

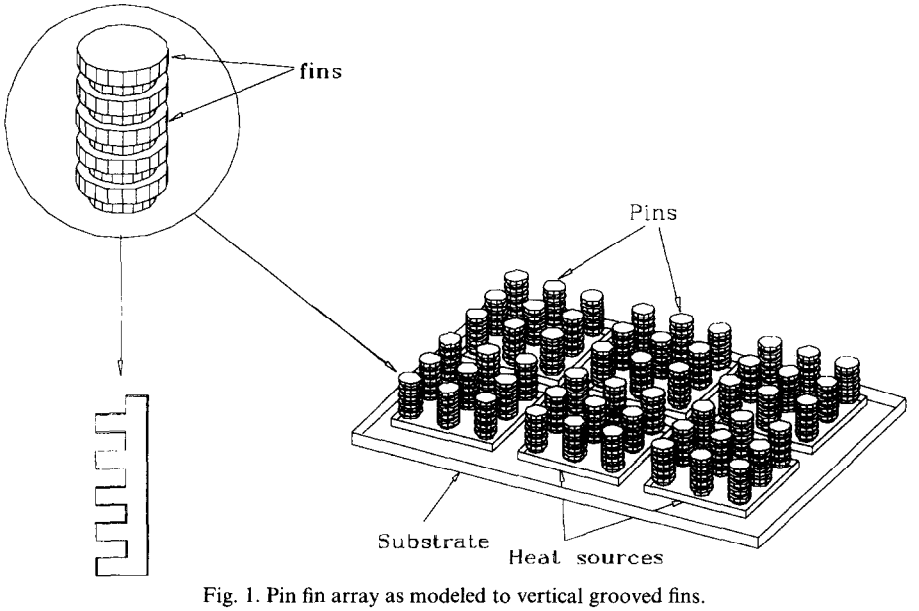

Fig. 1. Pin fin array as modeled to vertical grooved fins.

well with a new asymptotic limit with a 0.316 power dependence on the modified Rayleigh number based on the channel height. Shakerin *et al.* [6] studied natural convection in an enclosure with discrete roughness elements on a vertical heated wall and they reported that the total heat transfer rate may be nearly the same as for a smooth wall in spite of the increase surface area in the studied limits. Kang *et al.* [7] per-

formed an experimental study of natural convection from a heat source module mounted on a horizontal or vertical surface. The natural convection flow and the associated heat transfer characteristics were found to depend strongly on the rate of energy input and the source thickness. Bhavnani and Bergles [8] studied laminar natural convection heat transfer from a vertical flat plate with several transverse roughness elements (ribbed and stepped surface) using interferometer experiments. The experiments were performed varying the aspect ratio of rib and step. The performance of ribbed surfaces was below that of a plain plate of equal projected area in the tested Grashof number. The heat transfer rate decreased as the rib pitch-to-height ratio decreased. The heat transfer rate was larger in stepped surface than in ribbed surface. Desai *et al.* [9] investigated on natural convection in an enclosure with a cooled top wall and multiple protruding heaters using numerical simulation. A vertical side wall had five protrusions and the top wall functioned as the heats sink while the opposing vertical wall and the bottom wall were insulated. A secondary flow existed at the top of the enclosure. At low Rayleigh number ($Ra^* \leqslant 1.5 \times 10^7$), the flow was stable and characterized by the presence of a primary flow cell and a counter-rotating secondary cell at the top of the enclosure. At higher Rayleigh number ($Ra^* \geqslant 3 \times 10^8$), however, the isothermal top wall caused a periodic flow pattern in the enclosure.

The purpose of this study is to enhance heat transfer using vertical plate with several horizontal rectangular grooves for application to cooling of electronic components. Both of experimental and numerical researches were made to study natural convection from the grooves. A Mach–Zehnder interferometer was used to visualize the temperature distribution and the interferogram was compared with the numerical results using a modified SIMPLER code with pressure boundary condition.

EXPERIMENTAL STUDY

A model of the rectangular grooved fin is shown in Fig. 2. The thickness of the test section of 0.2 m. The fin has five rectangular protrusions and its surface is heated isothermally owing to very high thermal conductivity. Symbol H denotes the depth of the groove, W_1 is the width of the groove, W_2 is the width of the protruded top surface and W, the pitch length, is the sum of W_1 and W_2. The specimens were made of aluminum of a high thermal conductivity. Heating wire was uniformly attached on the backside of the specimen and it was heated using a DC power supply. To prevent heat dissipation from the backside, an insulation material was adhered. The experiments were performed varying the aspect ratios H/W and W_2/W. The actual sizes of the models are shown in Table 1.

The Mach–Zehnder interferometer used in the experiment is schematically shown in Fig. 3. Isothermal lines were visualized using infinite fringe frames and the distribution of Nusselt numbers at the surfaces was measured using finite fringe frames [10]. After we took a photograph of the interferogram with a camera, we magnified the picture to the size of $10'' \times 8''$. Then, we analyzed it with a digitizer having a 500 dpi (dots per inch) resolution. It was assumed, for the convenience of data processing, that the temperature gradient of the refractive index dn/dT was constant. For verification of the experimental results, the average Nusselt number over a vertical flat plate was measured and compared with the studies of Churchill and Chu [11]. There was about 5% discrepancy between them. The greatest error came from the uncertainties in reading the interferogram, i.e., the temperature gradient near the wall was very high and the fringes had fairly large thickness. Although additional effects such as three-dimensional flow were considered to exist, they were negligible compared with the reading error.

NUMERICAL STUDY

The interferograms give information only on the temperature distributions. To find the velocity field and to further verify the experimental results, numerical simulations were also performed.

The dimensionless governing equations are as follows:

$$\frac{\partial u^*}{\partial x^*} + \frac{\partial v^*}{\partial y^*} = 0 \tag{1}$$

$$u^* \frac{\partial u^*}{\partial x^*} + v^* \frac{\partial u^*}{\partial y^*} = \frac{\partial^2 u^*}{\partial x^{*2}} + \frac{\partial^2 u^*}{\partial y^{*2}} - \frac{\partial P^*}{\partial x^*} \tag{2}$$

$$u^* \frac{\partial v^*}{\partial x^*} + v^* \frac{\partial v^*}{\partial y^*} = \frac{\partial^2 v^*}{\partial x^{*2}} + \frac{\partial^2 v^*}{\partial y^{*2}} - \frac{\partial P^*}{\partial y^*} + Gr_w \theta \tag{3}$$

$$u^* \frac{\partial \theta}{\partial x^*} + v^* \frac{\partial \theta}{\partial y^*} = \frac{1}{Pr}\left(\frac{\partial^2 \theta}{\partial x^{*2}} + \frac{\partial^2 \theta}{\partial y^{*2}}\right). \tag{4}$$

The Boussinesq approximation was used by introducing $P = P^* \rho_\infty (v^2/W^2) - \rho_\infty g y$ and the employed dimensionless quantities were defined as:

$$x^* = \frac{x}{W}, \quad y^* = \frac{y}{W}, \quad u^* = \frac{uW}{\nu},$$

$$v^* = \frac{vW}{\nu}, \quad \theta = \frac{T - T_\infty}{T_w - T_\infty},$$

$$Gr_w = \frac{g\beta(T_w - T_\infty)W^3}{\nu^2} \quad \text{and} \quad Pr = \frac{\nu}{\alpha} \tag{5}$$

where symbol W is the length of a pitch $(W_1 + W_2)$.

The boundary conditions were given as follows:

$$u^* = 0, \quad v^* = 0 \quad \text{at the surfaces of the fin} \tag{6}$$

$$P^* = 0 \quad \text{at the top, bottom and right boundaries} \tag{7}$$

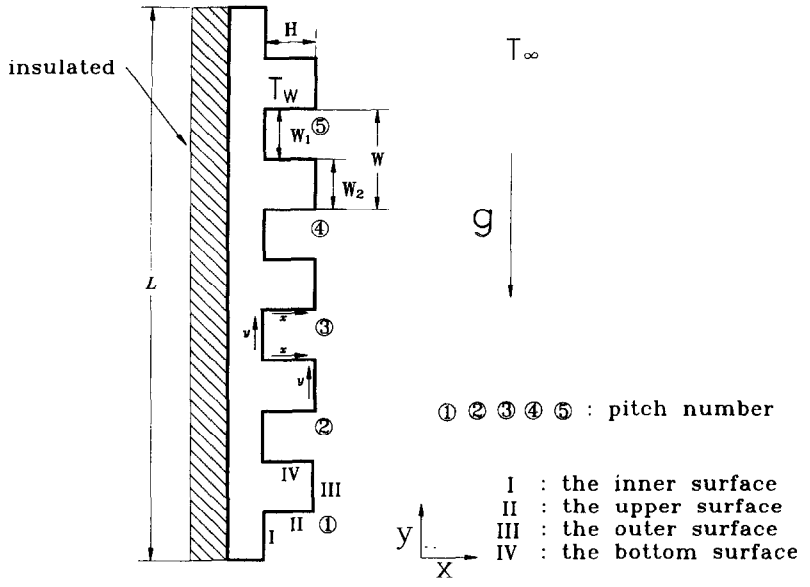

Fig. 2. Notations of the vertical rectangular grooved fin.

Table 1. Dimensions of the models

Case	$W = W_1 + W_2$ (mm)	H/W	W_2/W
1 (square groove)	14	0.5	0.5
2 (short groove)	14	0.25	0.5
3 (long groove)	14	1	0.5
4 (large groove)	15	7/15	0.2

$$\theta = 1 \quad \text{at the surface of the fin}$$

$$\frac{\partial \theta}{\partial x^*} = 0 \quad \text{at the right boundary.} \tag{8}$$

In equations (7) and (8), the right boundary is a far location which is twelve times the depth of a groove away from the fin. The top computational boundary is above the last protrusion and the bottom boundary is below the first.

When the Nusselt number and the relevant heat transfer rate are defined as follows,

$$Nu_w = \frac{hW}{k}$$

$$q'' = h(T_w - T_\infty) \tag{9}$$

they are dependent on the following variables from the governing equations and boundary conditions.

$$Nu_w = f(Gr_w, Pr, H/W, W_2/W, \ldots). \tag{10}$$

If the Prandtl number is constant, the above equation can be alternatively written as

$$Nu_w = f(Ra_w, H/W, W_2/W, \ldots) \tag{11}$$

where, $Ra_w = Gr_w \cdot Pr$.

The effect of Prandtl number was assumed to be negligible for common fluids. A constant Prandtl number 0.71 was taken, indeed. Thus, the effects of Ra_w and aspect ratios (H/W, W_2/W) were investigated in this study.

In a natural convections problem, velocities cannot be prescribed at the boundaries. We modified a SIMPLER code [12] for pressure boundary condition and used pressures as the boundary conditions (see the Appendix for details). Underrelaxation of boundary velocity and pressure is made to make the computation stable.

VERIFICATION OF THE NUMERICAL SIMULATION

First, grid dependence was examined to minimize the numerical uncertainty. The calculated variables using current grids (38×81) were compared with those using a 104×233 mesh. The difference of total heat transfer rate between them was at most about 3%. Compromising between the computational cost and the accuracy, the current mesh is considered appropriate.

Secondly, the average heat transfer rate for a vertical flat plate was computed and compared with that of Churchill and Chu [11]. Only about 3% discrepancy for the numerical result was found.

Lastly, to demonstrate the accuracy of numerical result, the local Nusselt number distribution in a groove of case 1 for $Ra_w = 1.14 \times 10^4$ is shown in Fig. 4 as compared with the interferometric result. Both results agree well with each other within 5% error. As mentioned earlier, however, the numerical results are slightly better in accuracy.

Furthermore, experimental and numerical isotherms are given in Fig. 5. Isotherms of experimental

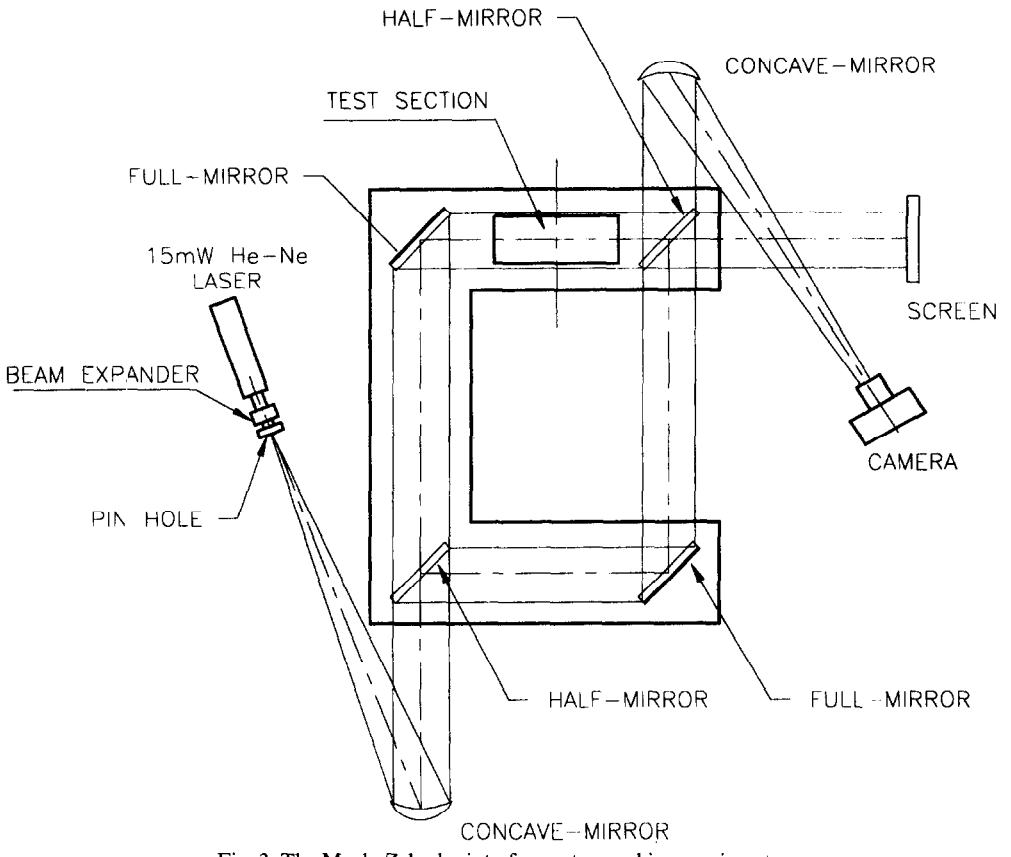

Fig. 3. The Mach–Zehnder interferometer used in experiments.

and numerical results agree very well both qualitatively and quantitatively. Since the numerical results are considered better in accuracy than the experimental results, quantitative evaluations hereafter are based on numerical results. All the four cases of Table 1 were calculated and the results are compared. Since the geometry is an important design parameter while the overall size is roughly fixed, the relative performances of different grooves need be discriminated by directly comparing the heat transfer rates. The Rayleigh number was varied by taking $Ra_w = 1.14 \times 10^4$, 1.14×10^5, 1.14×10^6 and 1.14×10^7.

RESULTS AND DISCUSSION

The isotherms for the four cases in Table 1 are shown in Fig. 6 when Ra_w is 1.14×10^4. Generally, the higher the location of the groove is, the thicker is the thermal boundary layer just like in a vertical flat plate. The outer parts of the protrusion have dense isotherms and those in the groove are sparse. The wall heat flux in the groove is thus much lower than that on top of the protrusion. Isothermal lines of cases 2 and 4 penetrate from the ambient into the groove more deeply than the other cases. For these two cases, the groove aspect ratio H/W_1 is smaller than the other cases. The local Nusselt numbers are shown in Fig. 7 for case 1 (square groove) with $Ra_w = 1.14 \times 10^4$. The local Nusselt numbers is the greatest at the outer surface (III) of the groove. At the bottom (IV) and upper surface (II), it increases from the inner corner to the outer edge. And the heat transfer rate at the top surface is higher than that at the bottom surface. At the inner surface (I) of the groove, it is very small. It has a local maximum at the center and decreases at the corners. And the larger the pitch numbering is (meaning the upper ones; see Fig. 2), the smaller is the local Nusselt numbers. The distribution pattern of Nusselt number for the other cases (2–4) is also similar. However, cases 2 and 4 have greater Nusselt number at the inner surface and case 3 has a smaller value there.

The pattern of Nusselt number distribution in the groove can be easily understood when the flow pattern in the groove is known. Streamlines of each case are shown in Fig. 8 for $Ra_w = 1.14 \times 10^4$. Note that the streamlines in the groove are drawn with very fine stream function interval. Indeed, velocities in the groove are very small. The streamlines in the groove vividly visualize the recirculations. A weak recirculation flow is generated near the bottom surface of the second groove and grows in its size in the following grooves while the main flow penetrates deep in the groove without a recirculation at the first one. The

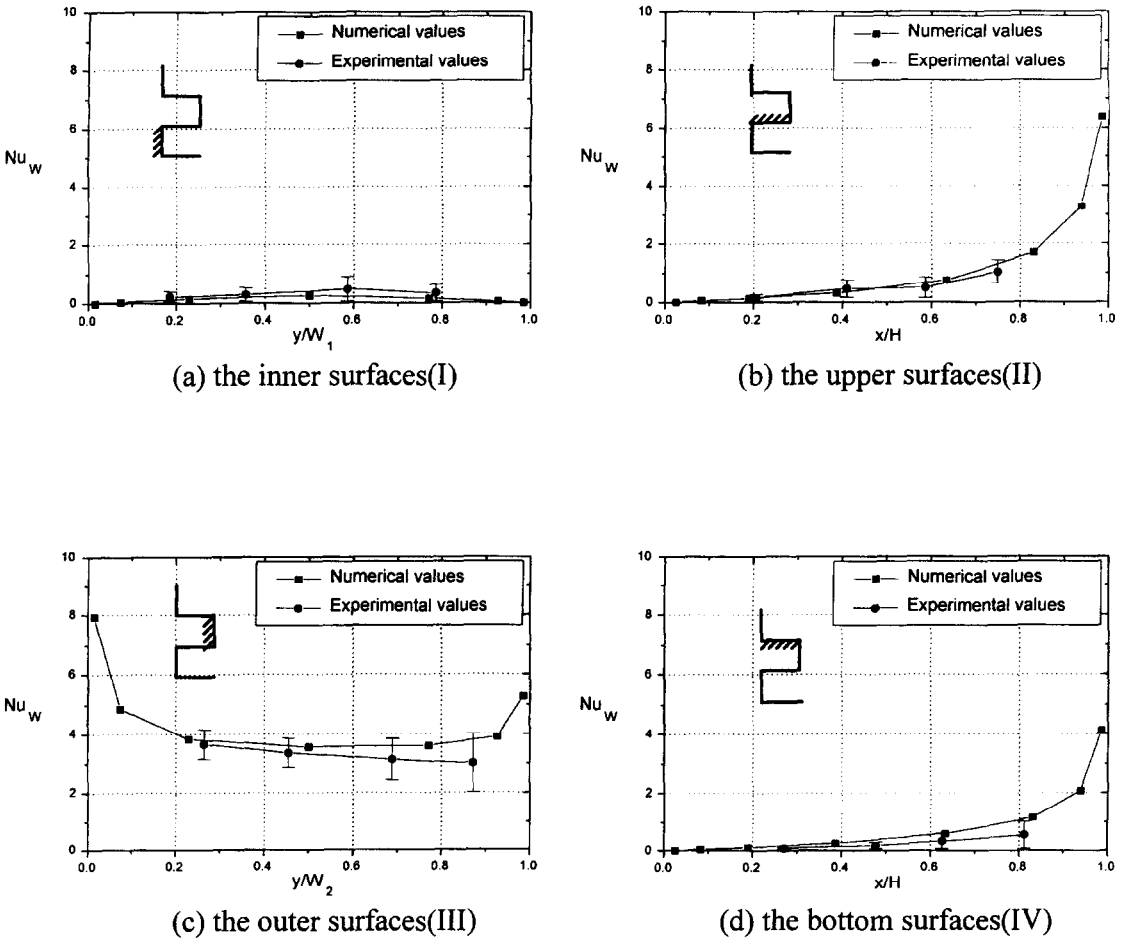

(a) the inner surfaces(I)

(b) the upper surfaces(II)

(c) the outer surfaces(III)

(d) the bottom surfaces(IV)

Fig. 4. Comparison of the experimental Nusselt numbers with error bars with the numerical ones at the surfaces of the third pitch for $Ra_w = 1.14 \times 10^4$ (case 1) (see Fig. 2 for the pitch and the surface numbering).

recirculations in the groove prevents the main flow from flowing into the groove. For this reason, the heat transfer rate at the bottom surface is very small and so is the Nusselt number. When the groove is very deep (see Fig. 8(c)), another recirculation is added in the groove and the Nusselt number at the bottom surface becomes even smaller.

For $Ra_w = 1.14 \times 10^4$, the total heat transfer rate is the largest for case 3 and its amount is about 25% larger than that of vertical flat plate. It is smaller in the sequence, case 1 (4.6%), case 2 (2.8%) and case 4 (−0.2%). The total heat transfer of case 4 is even smaller than that for a vertical flat plate although the exposed area is greater than that of flat plate. This finding is analogous to the findings of Shakerin *et al.* [6] and Bhavnani and Bergles [8].

The isotherms for $Ra_w = 1.14 \times 10^4$, 1.14×10^5, 1.14×10^6 and 1.14×10^7 in case 1 are shown in Fig. 9 to see the effect of Ra_w. The higher Ra_w is, the more deeply the isotherms and streamline penetrate into the groove. The ratio of contribution by the inner surface to the total heat transfer increases as Ra_w increases. The dimensionless total heat transfer rate for variation of Ra_w is shown in Table 2 for all cases and for a vertical flat plate. Total heat transfer rates of all cases are larger than that of a flat plate when $Ra_w \geqslant 1.14 \times 10^5$. The higher Ra_w is, the larger is the enhancement of heat transfer. Velocity in the groove is large at large Rayleigh number and heat transfer rates at the surfaces in the groove also become large. The advantage by increasing the surface area is visualized when the Rayleigh number is larger than about 10^6.

The correlations of Nusselt number vs. Rayleigh number for each pitch were calculated from the previous quantitative results. Symbol $\overline{Nu_1}$ is the average Nusselt number of the first pitch, which is the dimensionless heat transfer rate obtained by dividing the total heat transfer rate q_1 per unit depth from surfaces, I–IV of the first protrusion by $k(T_w - T_\infty)$, i.e.,

$$\overline{Nu_1} = \frac{q_1}{k(T_w - T_\infty)} \tag{12}$$

$$q_1 \bar{h}_1 W(T_w - T_\infty). \tag{13}$$

The correlations of Nu_1 vs. Ra_w are optimized as follows:

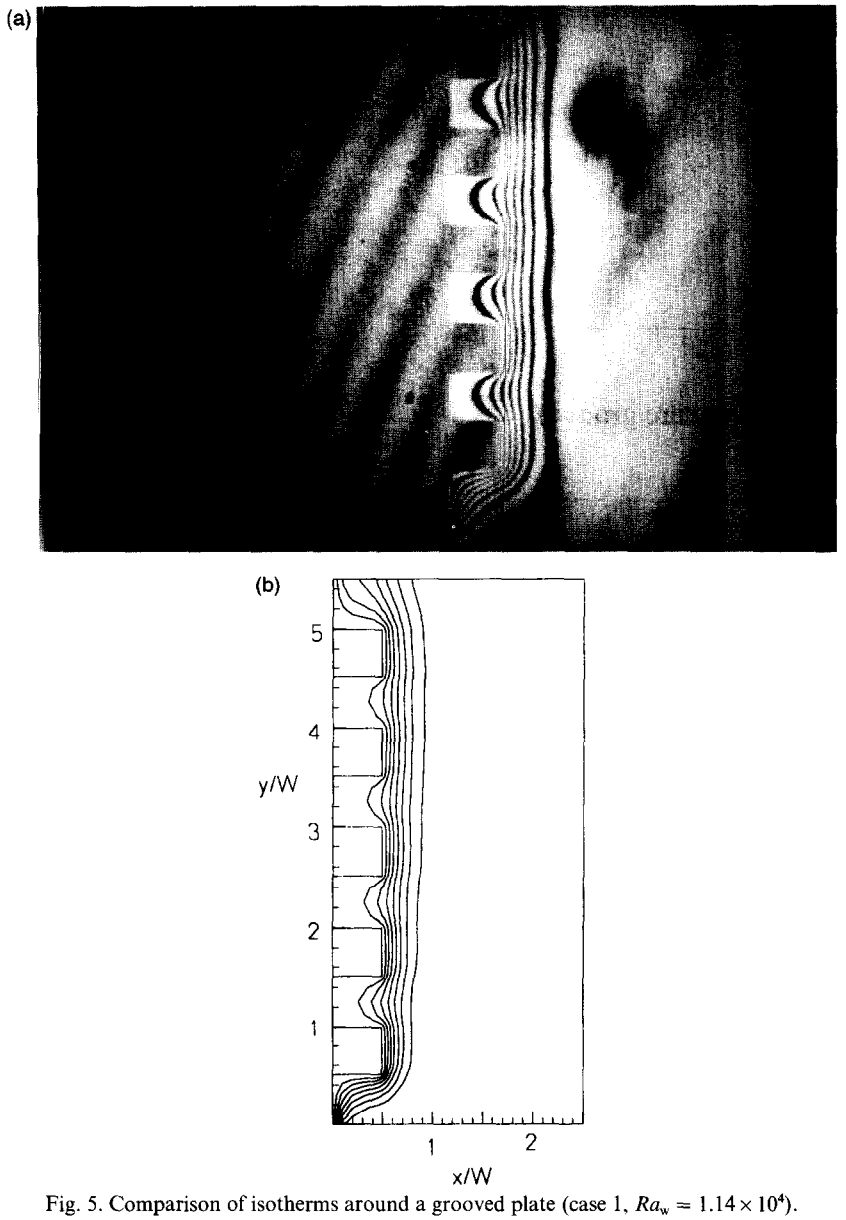

Fig. 5. Comparison of isotherms around a grooved plate (case 1, $Ra_w = 1.14 \times 10^4$).

$$\overline{Nu_1} = 0.45 Ra_w^{0.29} \quad \text{for case 1}$$
$$\overline{Nu_1} = 0.46 Ra_w^{0.28} \quad \text{for case 2}$$
$$\overline{Nu_1} = 0.45 Ra_w^{0.3} \quad \text{for case 3}$$
$$\overline{Nu_1} = 0.4 Ra_w^{0.3} \quad \text{for case 4.} \qquad (14)$$

With $\overline{Nu_i}$ denoting the average Nusselt number of the ith pitch, defined in the same manner as $\overline{Nu_1}$, the relation between $\overline{Nu_i}$ and $\overline{Nu_1}$ is correlated as follows:

$$\frac{\overline{Nu_i}}{\overline{Nu_1}} = \left[1 + \frac{(i-1)}{x_1}\right]^{-n} \qquad (15)$$

where x_1 is a correlation parameter. This is a vertical position from the base of the first pitch. It is contrived to correlate the average Nusselt number of first pitch with that of another pitch. The values of x_1 and n are shown in Table 3. The average error of these relations is about 6% in the given range of Ra_w. The relations are valid only when the number of pitches does not significantly exceed the tested case, i.e., five. Fortunately, many practical applications fall in this limitation.

The total heat transfer rate from a vertical rectangular grooved fin increases very rapidly with the increase of Ra_w, while the growth rate for a vertical flat plate is not that high. In equation (14), the average Nusselt numbers are proportional to the 0.28–0th power of Rayleigh number while that of a vertical flat plate is proportional to the 0.25th power of Rayleigh

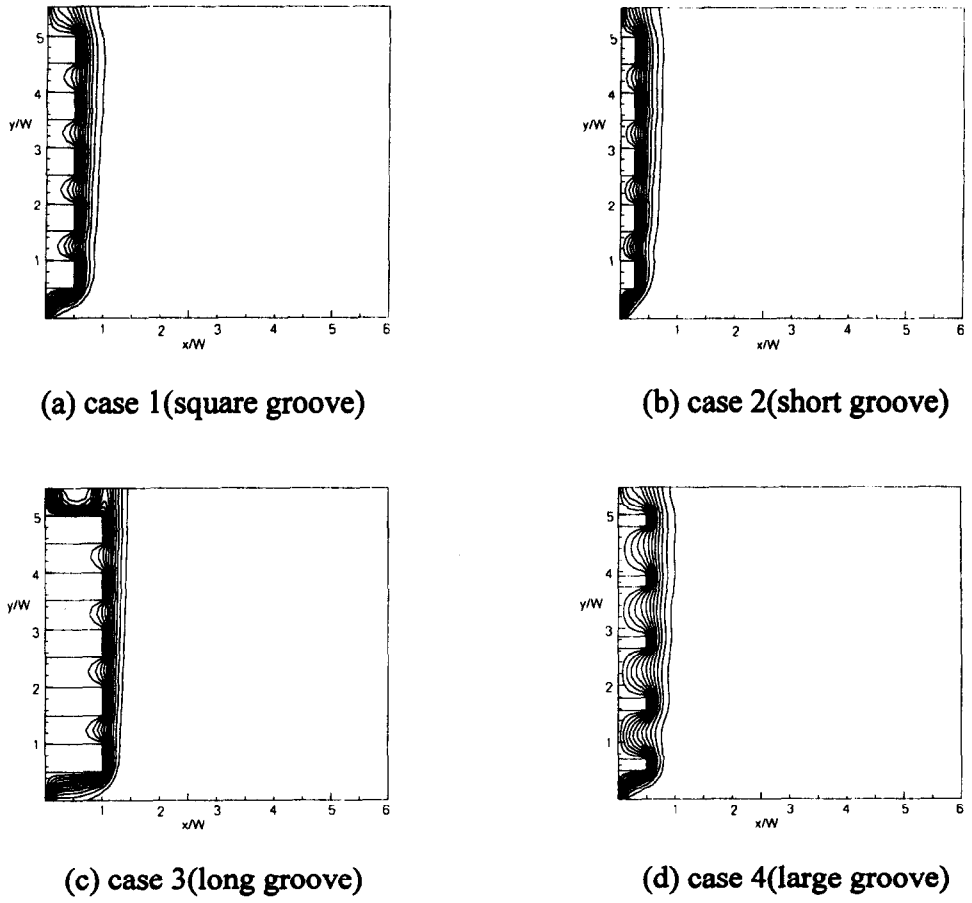

Fig. 6. Isotherms for the four geometries ($Ra_w = 1.14 \times 10^4$).

number. Apparently, the advantage of grooved fins is appreciable for larger Rayleigh numbers. The ratio of Nusselt numbers to the vertical flat plate case is arranged as:

$$\frac{\overline{Nu}_{\text{case1}}}{\overline{Nu}_{\text{flat}}} = 0.57 Ra_w^{0.061} \quad \text{for case 1}$$

$$\frac{\overline{Nu}_{\text{case2}}}{\overline{Nu}_{\text{flat}}} = 0.62 Ra_w^{0.051} \quad \text{for case 2}$$

$$\frac{\overline{Nu}_{\text{case3}}}{\overline{Nu}_{\text{flat}}} = 0.77 Ra_w^{0.046} \quad \text{for case 3}$$

$$\frac{\overline{Nu}_{\text{case4}}}{\overline{Nu}_{\text{flat}}} = 0.4 Ra_w^{0.094} \quad \text{for case 4.} \qquad (16)$$

The flow is laminar in the given range of Rayleigh number ($Ra_w < 1.14 \times 10^7$). But the flow field is found to become unstable when Ra_w is greater than 1.14×10^7.

The experiments and analyses here have been made for air ($Pr = 0.71$). For future application to liquid cooling, correlations for other fluids are desirable. At this point, no precise prediction for different Pr fluids can be made; however, it is anticipated that the present correlations for Nu here may be used for other fluids too within 25% error, since, for example for laminar natural convection along a vertical wall, the Nusselt number may be expressed as a function of Ra_w only for any Pr within 25% error [13].

CONCLUSION

Experimental and numerical studies on laminar natural convection from vertical plate with horizontal grooved fins have been performed. Both results agree well with each other for $Ra_w = 1.14 \times 10^4$ and the numerical method is further employed to investigate the heat transfer and flow field at different Ra_w. The Nusselt number is the greatest at the outer surface of the protrusion. At the bottom and top surfaces, it increases from the inner corner to the outer edge and it is a little higher at the top surface than at the bottom surface. It is very small at the inner surface; it has a local maximum at the center and decrease at the corner. At least one recirculation flow exists for all the tested cases near the bottom surface. It prevents the main flow from flowing into the grooves. Consequently, the total heat transfer rate from a grooved surface may be smaller than that from a smooth surface especially when the Rayleigh number is not large

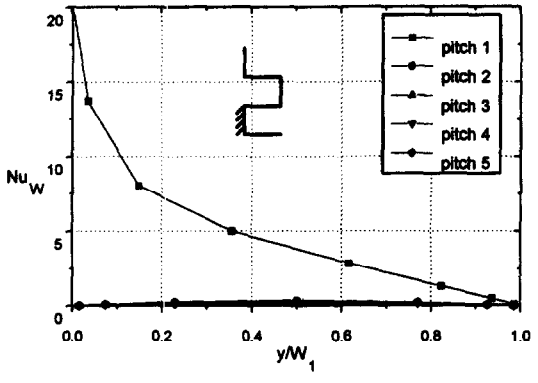

(a) the inner surfaces(I)

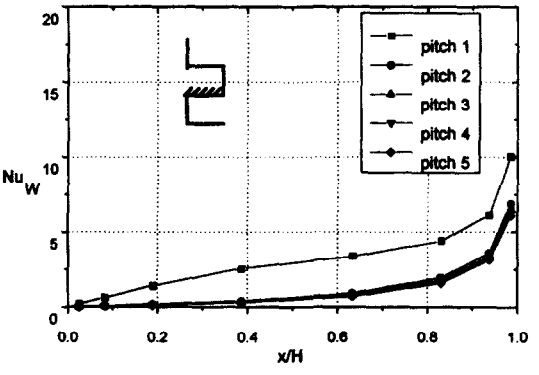

(b) the upper surfaces(II)

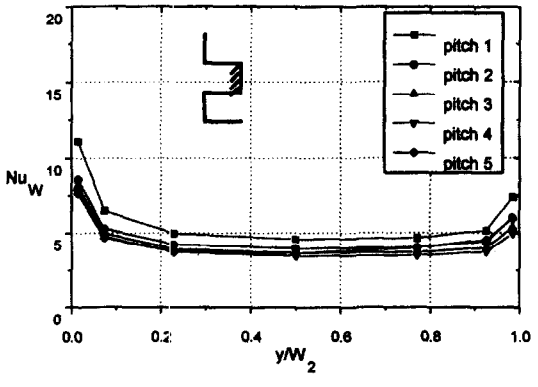

(c) the outer surfaces(III)

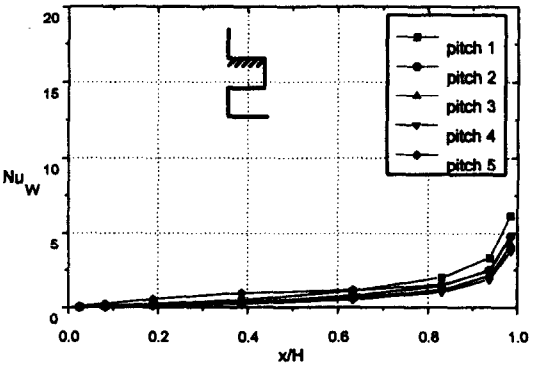

(d) the bottom surfaces(IV)

Fig. 7. Distribution of Nu_w at each surface of a pitch for $Ra_w = 1.14 \times 10^4$ (case 1) (see Fig. 2 for the pitch and surface numbering).

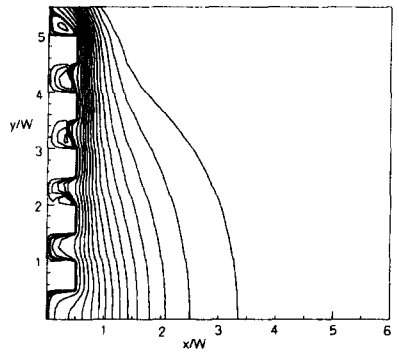

(a) case 1(square groove)

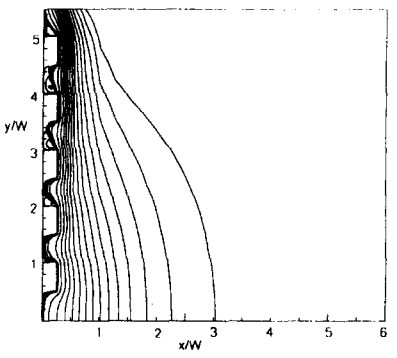

(b) case 2(short groove)

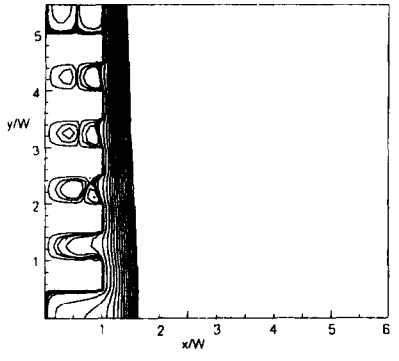

(c) case 3(long groove)

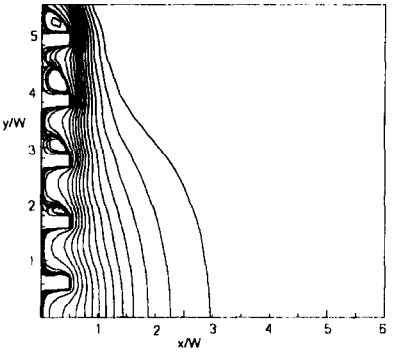

(d) case 4(large groove)

Fig. 8. Streamlines for the four geometries ($Ra_w = 1.14 \times 10^4$).

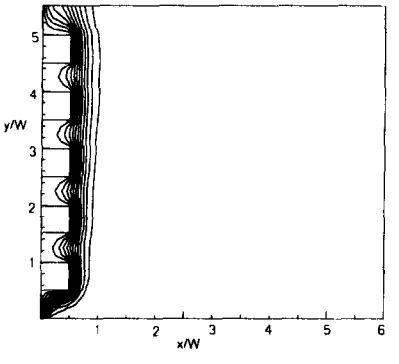

(a) Rayleigh number=1.14×10^4

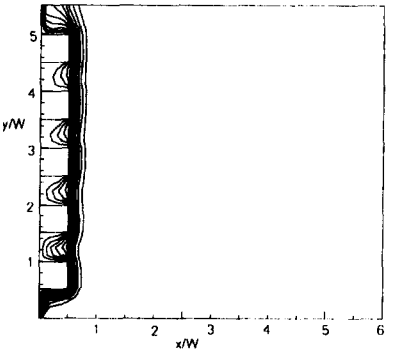

(b) Rayleigh number=1.14×10^5

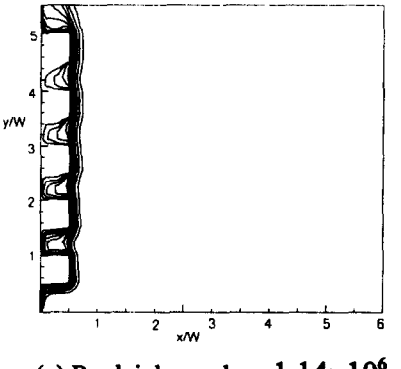

(c) Rayleigh number=1.14×10^6

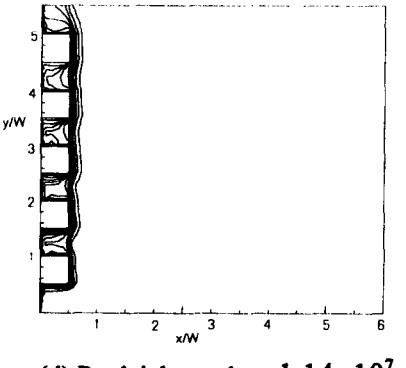

(d) Rayleigh number=1.14×10^7

Fig. 9. Isotherms when varying Ra_w (case 1).

Table 2. Dimensionless heat transfer rate for each case varying $Ra_w[Q/(k(T_w-T_\infty))]$

	$Ra_w = 1.14\times10^4$	$Ra_w = 1.14\times10^5$	$Ra_w = 1.14\times10^6$	$Ra_w = 1.14\times10^7$
Flat†	17.8	31.7	56.3	100.2
Case 1	18.62	34.86	72.66	158.4
Case 2	18.29	33.6	68.18	145.1
Case 3	22.29	39.38	79.37	171.5
Case 4	17.77	36.23	79.25	191.77

† These values were computed from the correlation of Churchill and Chu [11].

Table 3. The value of variables in equation (15)

	$Ra_w = 1.14\times10^4$		$Ra_w = 1.14\times10^5$		$Ra_w = 1.14\times10^6$		$Ra_w = 1.14\times10^7$	
	x_1	n	x_1	n	x_1	n	x_1	n
Case 1	0.0109	0.171	0.0205	0.21	0.106	0.299	0.342	0.365
Case 2	0.0281	0.197	0.0448	0.224	0.122	0.279	0.177	0.274
Case 3	0.00267	0.144	0.0053	0.188	0.0585	0.302	0.346	0.447
Case 4	0.15	0.29	0.985	0.596	0.506	0.376	0.51	0.161

enough. When Ra_w is large, the heat transfer rate from the governed fin becomes greater than that from a flat surface. The average Nusselt number of the first protrusion is roughly proportional to the 0.28–0.3th power of the Rayleigh number while that of a vertical flat plate is proportional to the 0.25th power of the Rayleigh number.

Proper correlations have been made to obtain the heat transfer rate from each pitch for the tested geometries and Rayleigh numbers.

Acknowledgements—The authors are grateful to Korea Science Foundation (Grant no. KOSEF 93-0600-02-3) and to Korean Ministry of Science and Technology for their financial support.

REFERENCES

1. Rymaszewski, E. J. and Tummala, R. R., Microelectronics packaging—an overview, in *Microelectronics Packaging Handbook*. von Nostrand Reinhold, New York, 1989.
2. Incropera, F. P., Convection heat transfer in electronic equipment cooling. *ASME Journal of Heat Transfer*, 1988, **110**, 1097–1111.
3. Chu, R. C. and Simons, R. E., Recent development of computer cooling technology. *The 6th International Symposium on Transport Phenomena*. Seoul, Korea, 1993, pp. 17–25.
4. Fujii, T. and Imura, H., Natural convection heat transfer from a plate with arbitrary inclination. *International Journal of Heat and Mass Transfer*, 1972, **15**, 755–767.
5. Hung, Y. H. and Shiau, W. M., Local steady-state natural convection heat transfer in vertical parallel plates with a two-dimensional rectangular rib. *International Journal of Heat and Mass Transfer*, 1988, **31**(6), 1279–1288.
6. Shakerin, S., Bohn, M. and Loehrke, R. I., Natural convection in an enclosure with discrete roughness elements on a vertical heated wall. *International Journal of Heat and Mass Transfer*, 1988, **31**, 1423–1430.
7. Kang, B. H. and Jaluria, Y., Natural convection heat transfer characteristics of a protruding thermal source located on horizontal and vertical surfaces. *International Journal of Heat and Mass Transfer*, 1990, **33**, 1347–1357.
8. Bhavnani, S. H. and Bergles, A. E., Effect of surface geometry and orientation on laminar natural convection heat transfer from a vertical flat plate with transverse roughness element. *International Journal of Heat and Mass Transfer*, 1990, **33**(5), 965–981.
9. Desai, C. P., Vafai, K. and Keyhani, M., On the natural convection in a cavity with a cooled top wall and multiple protruding heaters. *ASME Journal of Electronic Packaging*, 1995, **117**, 34–45.
10. Hauf, W. and Grigull, U., Optical methods in heat transfer. *Advance in Heat Transfer*. Academic Press, New York, 1970, **6**, 191–278.
11. Churchill, W. W. and Chu, H. H. S., Correlating equations for laminar and turbulent free convection from a vertical plate. *International Journal of Heat and Mass Transfer*, 1975, **18**, 1323–1329.
12. Patankar, S. V., *Numerical Heat Transfer and Fluid Flow*. Hemisphere Publishing Co., New York, 1980.
13. Burmeister, L. C., *Convective Heat Transfer*, 2nd edn. John Wiley and Sons, New York, 1993

APPENDIX—TREATMENT OF PRESSURE BOUNDARY FOR SIMPLER CODE

The further details of the modified SIMPLER code [12] for pressure boundary condition as follows.

Refer to ref. [12] for explanation of symbols in this Appendix.

Consider the conditions at $u(2,j)$ in Fig. A1 which is subject to pressure boundary condition. We take a very small control volume size at the boundary.

Equation for u_e

From SIMPLER algorithm,

$$a_e u_e = \sum_{\text{all but } w} a_{nb}u_{nb} + a_w u_w + b + (p_P - p_E)A_e. \quad \text{(A1)}$$

We can rewrite equation (A1) as

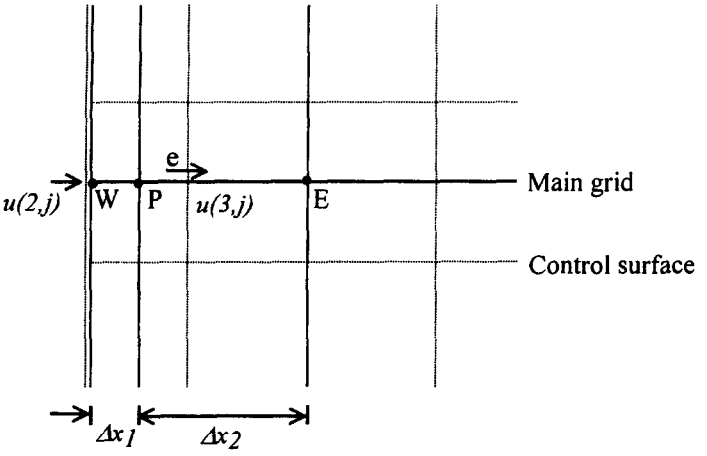

Fig. A1. Grids near the pressure boundary.

$$(a_e - a_w)u_e = \sum_{\text{all but } w} a_{nb}u_{nb} + a_w(u_w - u_e) + b + (p_P - p_E)A_e. \tag{A2}$$

With relaxation factor r, we perform equation (A1) $\times$ $(1-r)$ + equation (A2) $\times r$ to give

$$(a_e - ra_w)u_e = \sum_{\text{all but } w} a_{nb}u_{nb} + (1-r)a_w u_w + ra_w(u_w - u_e) + b + (p_P - p_E)A_e. \tag{A3}$$

We treat $a_e - ra_w$ as the new a_e, $(1-r)a_w$ as the new a_w and $b + ra_w(u_w - u_e)$ as the new b. The converged solutions of equations (A1), (A2) and (A3) are identical to each other regardless of the value of r, once they converge. If r is small, convergence is slower and stable.

Equation for pressure

The pressure equations for the near-boundary nodes are considered here. We have,

$$u_e = \hat{u}_e + d_e(p_P - p_E). \tag{A4}$$

Equation for u_w is conceived as follows. We assume,

$$u_w = \hat{u}_w + d_e\frac{\Delta x_2}{\Delta x_1}(p_W - p_P). \tag{A5}$$

Note that $\hat{u}_w$ is not known and $d_e(\Delta x_2/\Delta x_1)$ is made so as to get the pressure gradient. With equation (A5), a_W for p_P-equation becomes

$$a_W = a_E\frac{\Delta x_2}{\Delta x_1}. \tag{A6}$$

In evaluating b, $\hat{u}_w$ must be properly decided. Consider a case where $p_S = p_N = p_P$. Conduction-like pressure distribution is desirable to have $b = 0$. This means we should take $\hat{u}_e = \hat{u}_w$. However, direct application of this condition and equation (A6) makes the numerical scheme extremely unstable. Thus, equation (A5) is used to evaluate the following left-hand side appearing in the expression of b, as

$$\rho_w\hat{u}_w\Delta y_w - \rho_e\hat{u}_e\Delta y_e = \rho_w\hat{u}_w\Delta y_w - \rho_e\Delta y_e\left\{u_w - d_e\frac{\Delta x_2}{\Delta x_1}(p_W - p_P)\right\}. \tag{A7}$$

However, if we introduce this expression into the p_P-equation, we have $a_w p_P - a_w p_W$ in the constant term b, thus, the converged solution becomes independent of p_W. To avoid this, $(\Delta x_2/\Delta x_1)(p_w - p_P)$ is replaced by $p_P - p_E$, enforcing linear pressure distribution. Thus, in evaluating b,

$$\hat{u}_w = u_w - (p_P - p_E)d_e. \tag{A8}$$

This is equivalent to taking a_E twice the original value indirectly. This indirect scheme is retained, since direct doubling of a_E makes the computation very unstable. If the pressure boundary is an outlet, the static pressure there is the ambient (given) pressure. However, if it is an inlet, the ambient pressure most likely acts as a stagnation pressure. Thus, it is more realistic to assign the inlet static pressure by subtracting the dynamic head from the ambient pressure.

Equation for pressure correction

Like in the above paragraph, we take

$$u_w = u_w^* + d_w(p'_W - p'_P). \tag{A9}$$

Since p'_W is given p'_W is equal to zero.

Since we do not know d_w, we assume, as before, $d_w = d_e\Delta x_2/\Delta x_1$. This results in the same coefficients as the pressure equations (a_{nb} and a_P).

The modifications are summarized as: first, the constant term b in the discretization equation is different; second, boundary values are different (i.e. $p = p_{given}$ and $p' = 0$, respectively); and, last, u_w is also corrected using equation (A9). The last action makes the mass balance fully met.